Electronic Supplementary Material (ESI) for Physical Chemistry Chemical Physics.

Supporting Information for

Atomically Mixed Fe-Group Nanoalloys: Catalyst Design for the Selective Electrooxidation of Ethylene Glycol to Oxalic Acid

Takeshi Matsumoto,[a,b] Masaaki Sadakiyo,[a,b] Mei Lee Ooi,[a,b]
Tomokazu Yamamoto,[b,c] Syo Matsumura,[b,c] Kenichi Kato,[b,d]
Tatsuya Takeguchi,[b,e] Nobuki Ozawa,[b,f] Momoji Kubo,[f]
and Miho Yamauchi[1,2,]*

[a]International Institute for Carbon-Neutral Energy Research (WPI-I^{2}CNER), Kyushu University, Motooka 744, Nishi-ku, Fukuoka 819-0395, Japan.

[b]CREST, JST, 4-1-8 Honcho, Kawaguchi, Saitama 332-0012, Japan.

[c]Department of Applied Quantum Physics and Nuclear Engineering, Kyushu University, Motooka 744, Nishi-ku, Fukuoka 819-0395, Japan.

[d]RIKEN SPring-8 Center, 1-1-1 Kouto, Sayo-cho, Sayo-gun, Hyogo 679-5148, Japan.

[e]Department of Chemistry and Bioengineering, Faculty of Engineering, Iwate University, 4-3-5 Ueda, Morioka, Iwate 020-8551, Japan.

[f]Fracture and Reliability Research Institute, Graduate School of Engineering, Tohoku University, 6-6-11 Aoba, Aramaki, Aoba-ku, Sendai 980-8579, Japan.

* Correspondence to: E-mail: yamauchi@i2cner.kyushu-u.ac.jp.
Phone and Fax: +81-92-802-6874.

Contents

1. General procedures, syntheses, measurements, calculations

1-1. **Preparation of Fe-group Binary NA (FeCo/C, FeNi/C, and CoNi/C) and Monometallic NP (Co/C and Ni/C) Catalysts.** The synthetic operations were carried out as described in the manuscript. The scales of starting materials, reagents, and solvents used for preparations of NA and NP catalysts are summarized in Table S1.

Table S1. Scales of starting materials, reagents, and solvents

	FeCo/C	**FeNi**/C	**CoNi**/C	**Co**/C	**Ni**/C
A	0.3479	0.3480	0	0	0
B	2.0	2.0	0	0	0
C	0.3543	0	1.4163	0.708	0
D	2.0	0	8.0	4.0	0
E	0	0.4976	1.9978	0	3.9819
F	0	2.0	8.0	0	16
G	1.7623	1.7621	7.0483	1.7618	7.0487
H	200	200	200	200	200
I	30	20	40	30	40
J	0.3447	0.2793	0.9423	0.2358	0.9397
K	15	15	30	15	40
L	1.5128	1.5128	6.0528	1.5135	6.0534
M	300	300	300	300	300
N	300	300	0	0	0
O	1.0	0.87	3.6	0.7	2.7

1-2. **Powder X-ray diffraction (XRD) measurement.** Powder X-ray diffraction measurements were carried out with Cu Kα radiation (λ = 1.54059 Å) using a Rigaku SmartLab diffractometer at room temperature. Synchrotron powder XRD measurements were performed at the RIKEN materials science beamline BL44B2 of SPring-8.[1] The data was acquired using a Debye-Scherrer camera equipped with an imaging plate as an X-ray detector. The incident wavelength was 0.579057 Å for all Fe-group NA or monometallic NP samples, which were obtained by calibration using CeO_2 as a standard powder sample. The X-ray beam was collimated by a double slit of 0.5 mm by 3.0 mm. Powder samples of all Fe-group NA or monometallic NP were sealed in borosilicate glass capillaries in vacuo. The samples were irradiated by X-ray at 300 K. Figures S4 and S6 show the XRD patterns of **FeCoNi**/C, **FeCo**/C, **FeNi**/C, **CoNi**/C, **Fe**/C, **Co**/C, and **Ni**/C, respectively (black line), with Rietveld profiles (red line). The determined structural parameters are listed in Table S4.

1-3. **TEM measurement of Fe/C, Co/C and Ni/C monometallic NP catalysts.** TEM images of **Fe**/C, **Co**/C, and **Ni**/C were taken with a JEM-2010HCKM operated at 200 kV, and the obtained images are shown in Figure S5. For the measurements, **Fe**/C, **Co**/C, and **Ni**/C mounted on copper grids were prepared using similar procedures to those for **FeCo**/C, **FeNi**/C, and **CoNi**/C for BF-STEM image measurements.

1-4. **Cyclic voltammetry (CV) measurements using catalyst-modified electrodes.** The ethylene glycol (EG, 0.3 mg, Wako) suspension of prepared catalysts (10 mg) was applied on carbon felt (KRECA Paper, 4 cm^2, Kureha). The carbon felt was used in all experiments after washing with acetone three times and drying in vacuo overnight (about 12 h). As the counter electrode, coiled Pt wire was used. An Hg/HgO reference electrode (RE-6A, BAS Co. Ltd.) filled with 1 M KOH aqueous solution was used. All potentials were measured against this Hg/HgO reference, which has a potential of 0.098 V vs. the normal hydrogen electrode (NHE), and were finally converted to that vs. referenced hydrogen electrode (RHE). For CV using a prepared catalyst, a VersaSTAT 4 potentiostat (Princeton Applied Research, AMETEC Inc.) was used, applying the abovementioned three electrodes. A sample vial (100 mL in volume, ALS Co. Ltd.) equipped with a gas-tight Teflon cap was used. The electrolyte aqueous solution (80 mL, 20wt% KOH, 30wt% EG) was introduced, and the working, reference, and counter electrodes were placed inside the vial. The electrolyte solution was prepared by using ultrapure water (DIRECT-Q® 3UV, Millipore Corp., Merck Ltd.). After the Teflon cap was tightly closed, N_2 gas was bubbled in the cell for 30 min in order to purge the air from inside the cell. After deaeration, the current value was recorded against the applied potential using a 10 mV/s scan rate and 10 scan cycles. CV measurement of the blank was carried out using the same procedures as mentioned above except for using electrolyte solution (80 mL, 20wt% KOH).

1-5. **Chronoamperometry (CA) measurements using catalyst-modified anodic electrodes.** The EG (0.7 mg) suspension of prepared catalysts (50 mg) was applied on the carbon felt (4 cm^2 × 4, 16 cm^2 total). The carbon felt was fixed to a handmade stainless steel clip, and was used as the working electrode. All potentials were measured against vs. Hg/HgO and converted to values vs. RHE. For chronoamperometry measurements, a VersaSTAT 4 potentiostat was used, applying the abovementioned three electrodes. The electrochemical experiments were fully carried out inside the glove box filled with N_2 gas. A home-built double compartment cell, where each compartment is separated by a proton-conducting membrane (Nafion®, NRE-212, Sigma-Aldrich) and equipped with gas-tight Teflon caps was used. For the anodic cell (75 mL in volume), electrolyte aqueous solution (50 mL, 20wt% KOH, 30wt% EG) and a stirring bar were introduced, and the working and reference electrodes were immersed. On the other hand, for the cathodic cell (75 mL in volume), electrolyte aqueous solution (50 mL, 20wt% KOH) and a stirring bar were introduced, and a counter electrode was fixed to the cap. Both electrolyte solutions were prepared using ultrapure water. After the Teflon caps were tightly closed, N_2 gas was bubbled in both the anodic and cathodic cells for 30 min in order to purge the air from the cells. The headspace of the anodic cell was connected to the gas chromatograph (GC) (7890A, Agilent Technologies, Inc.) equipped with packed columns (HayeSep Q 0.5 m, MS5A 6 ft, HayeSep Q 6 ft, Agilent Technologies, Inc.), thermal conductivity detector (TCD), and flame ionization detector (FID). The configuration of devices is described in our previous report.[2] Solution samples (50 μL) were collected from both anodic and cathodic cells at 0 and 125 min and analyzed by using HPLC (Shimadzu LC-20AD, 50 mM $HClO_4$ aqueous solution carrier) equipped with a refractive index detector (RID-10A) and diode array detector (SPD-M20A) for determination of generated oxide species of EG, i.e., oxalic acid, glycolic acid, formic acid, and formaldehyde, etc.

1-6. **Definition of number of electrons, current efficiency, and selectivity.**

Number of Electrons. The number of electrons is defined as the number of electrons that are related to the oxidized product formation from EG. The number of electrons was calculated from the amount of an oxidized product, which was quantified by HPLC, from the reaction solution in the anodic cell. For example, 8 electrons are required for oxalic acid formation from EG. Therefore, if *x* mol of oxalic acid was detected during the reaction, the "number of electrons" for oxalic formation can be calculated using the equation below (Eq. 1).

$$\text{Number of Electrons for Oxalic Acid} = x \times 8 \qquad \text{Eq. 1}$$

The number of electrons was finally divided by the metal weight in the catalyst, and shown as per metal weight (g) in Figures 3a and S10, 11, respectively.

Current Efficiency. The current efficiency is defined as the percentage of the electrons, which is relevant to the product formation, out of the total number of electrons that pass through the circuit and are counted by the potentiostat during the experiment. This value can be calculated from the "number of electrons" and "Coulomb number" counted by the potentiostat, using the equation described below (Eq. 2). If this value is close to 100 (%), the counted electrons can be considered to be based on the EG oxidation, i.e., oxidized product formation from EG. In contrast, when it is close to 0 (%), the counted electrons are based on another factor, e.g., catalyst self-oxidation.[3]

$$\text{Current Efficiency (\%)} = \frac{\text{Number of Electrons} \times \text{Faraday Constant}}{\text{Counted Coulomb Number}} \times 100 \qquad \text{Eq. 2}$$

Selectivity. The selectivity is defined as the percentage of electrons related to the specific product formation out of the total electrons for all product formation. This value can be calculated from the "number of electrons" for a specific product and the sum of them for all products. For example, "selectivity" of oxalic acid can be calculated using the equation below (Eq. 3).

$$\text{Selectivity (\%) of Oxalic Acid} = \frac{\text{Number of Electrons for Oxalic Acid}}{\text{Number of Electrons for All the Products}} \times 100 \qquad \text{Eq. 3}$$

1-7. Computational method.

The first-principles calculations were performed using Accelrys DMol[3] code[4], in which effective core potentials for the core electrons, the double numerical plus polarization basis sets for the atomic orbitals, and generalized gradient approximation using the Perdew-Burke-Ernzerhof functional[5] were applied. All calculations were performed with the two-dimensional Brillouin zone sampled by 4 x 4 x 1. Considering crystal structures of NAs, i.e., **FeCoNi** and **FeCo** NAs have fcc and bcc structures, periodically repeated slabs of three atomic layers were used for the **FeCo**(001) and **FeCoNi**(111) surface models. The surface size of **FeCo**(001) and **FeCoNi**(111) is 11.43 Å x

11.43 Å and 7.53 Å x 13.04 Å, respectively. All atoms positions of the slab were fixed. At the adsorption process, one O-H bond of glycolic acid was dissociated due to ionization by alkaline solvent. Here, for neutralization of the model, a hydrogen atom is set at bottom of the slab.

2.

Table S2. Catalytic systems for EG electrooxidation.

Catalyst	Conditions	Current Efficiencies or Selectivity (%)			Ref.
		Glycolic Acid (Glycolate)	Oxalic Acid (Oxalate)	Formic Acid (Formate)	
FeCoNi/C	20wt% KOH 30wt% EG 0.4 V (vs. RHE)	36.0[a]	43.5[a]	0[a]	This Work
PtNiSnO$_2$/C	1 mol/dm^3 KOH 0.5 mol/dm^3 EG 0.5 V (vs. RHE)	80[a]	< 7[a]	13[a]	6
Pt/C	2.0 M KOH 1.0 M EG 0.5 V (vs. RHE)	95[b]	1.3[b]	3.7[b]	7
Pd(NiZn)/C	2.0 M KOH 5.0wt% EG after DEGFC testing (const. 20 mA cm^{-2})	55.4[a]	37.6[a]	0[a]	8

a. Current efficiency, *b*. Selectivity

Reported results regarding the EG electrooxidation are tabulated in Table S2. The current efficiency and product selectivity are discussed in only three reports. The other reports for EG electrooxidation catalyst are listed as reference numbers of [9-43].

3.

Table S3. Chemical composition of Fe-group NA and monometallic NP catalysts.

	FeCoNi/C[a]	**FeCo**/C	**FeNi**/C	**CoNi**/C	**Fe**(bcc)/C[a]	**Fe**(fcc)/C[a]	**Co**/C	**Ni**/C
Metal content / wt%								
	38.1	38.3	40.1	37.0	28.5		48.2	46.3
Molar ratio / %[b]								
Fe	33.4	45.7	47.3	-	100		-	-
Co	36.9	54.3	-	49.2	-		100	-
Ni	29.7	-	52.7	50.8	-		-	100
Composition ratio / %[c]								
Fe	33.3	50	50	-	100		-	-
Co	33.3	50	-	50	-		100	-
Ni	33.3	-	50	50	-		-	100

a: see Ref. 2, *b*: obtained by ICP-MS, *c*: composition ratio at the synthesis steps.

4.

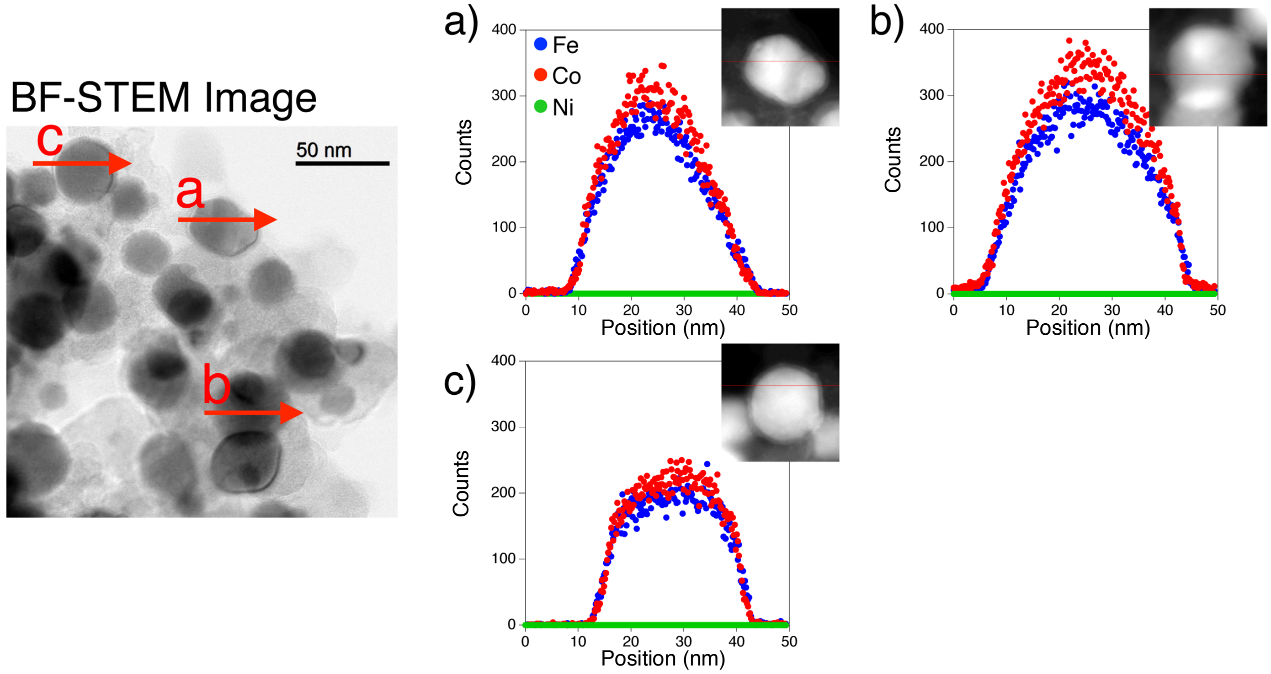

Fig. S1. Line profiles for **FeCo**/C shown in BF-STEM image (left). Targeted particles were randomly selected and marked with arrows (a-c). Scans were performed along lines marked as a-c in the BF-STEM image on the left. The line intensity of characteristic X-rays, such as Fe-Kα, Co-Kα and Ni-Kα, from the targeted particle is indicated with blue, red, and green dots, respectively. Insets: HAADF images of the selected particles.

5.

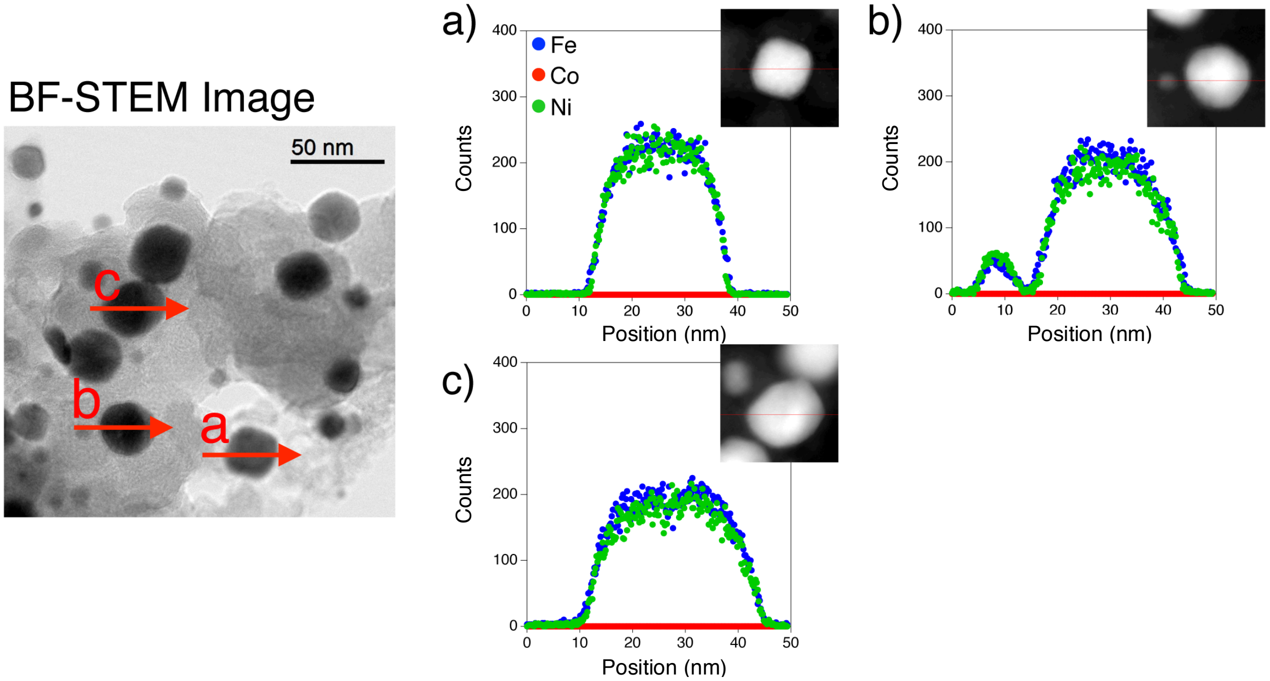

Fig. S2. Line profiles for **FeNi**/C shown in BF-STEM image (left). Targeted particles were randomly selected and marked with arrows (a-c). Scans were performed along lines marked as a-c in the BF-STEM image on the left. The line intensity of characteristic X-rays, such as Fe-Kα, Co-Kα and Ni-Kα, from the targeted particle is indicated with blue, red, and green dots, respectively. Insets: HAADF images of the selected particles.

6.

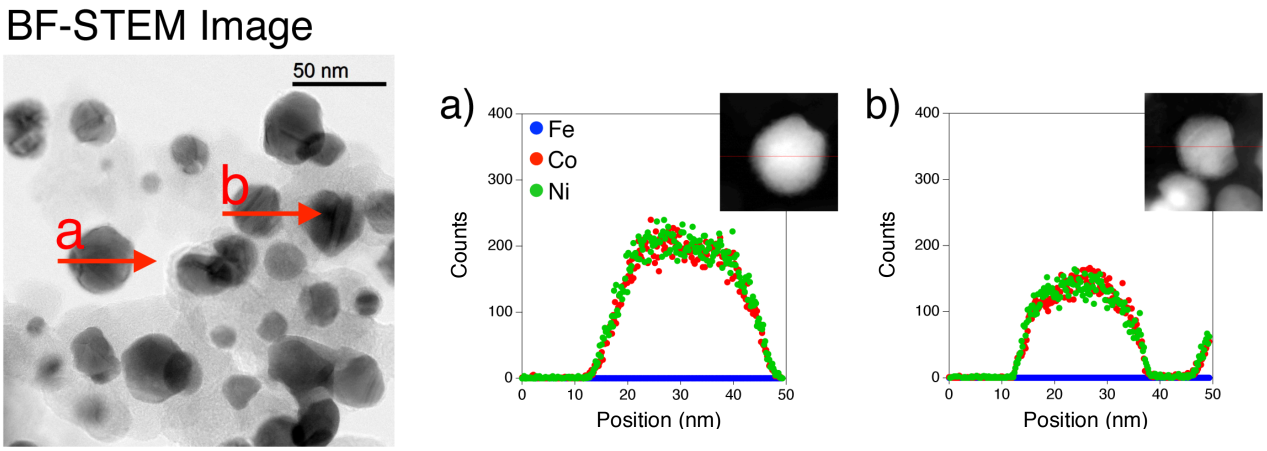

Fig. S3. Line profiles for **CoNi**/C shown in BF-STEM image (left). Targeted particles were randomly selected and marked with arrows (a and b). Scans were performed along lines marked as a and b in the BF-STEM image on the left. The line intensity of characteristic X-rays, such as Fe-Kα, Co-Kα and Ni-Kα, from the targeted particle is indicated with blue, red, and green dots, respectively. Insets: HAADF images of the selected particles.

7.

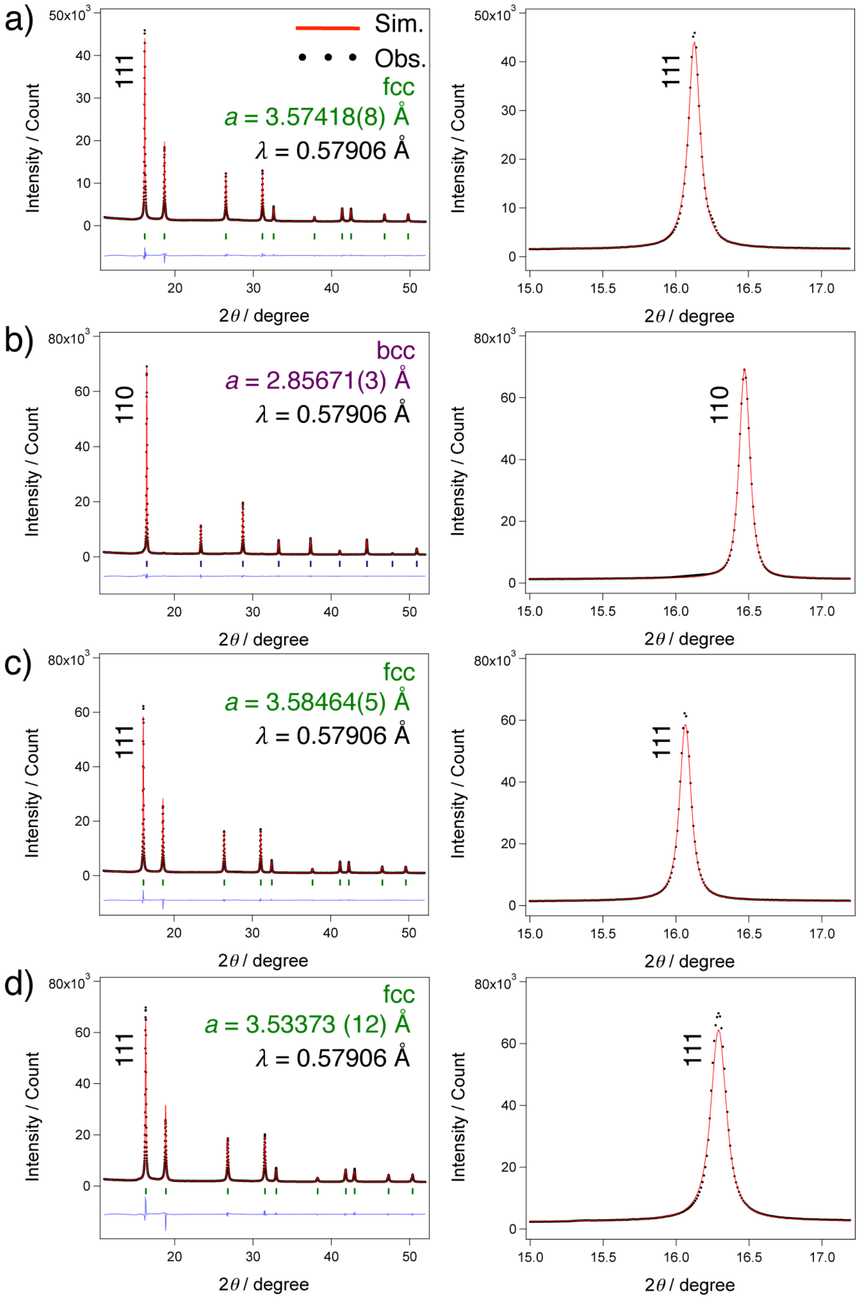

Fig. S4. Powder XRD patterns (black) of (a, left) **FeCoNi**/C, (b, left) **FeCo**/C, (c, left) **FeNi**/C, and (d, left) **CoNi**/C and optimized Rietveld profiles (red), with (right) close-up patterns around the lowest angle peaks.

8.

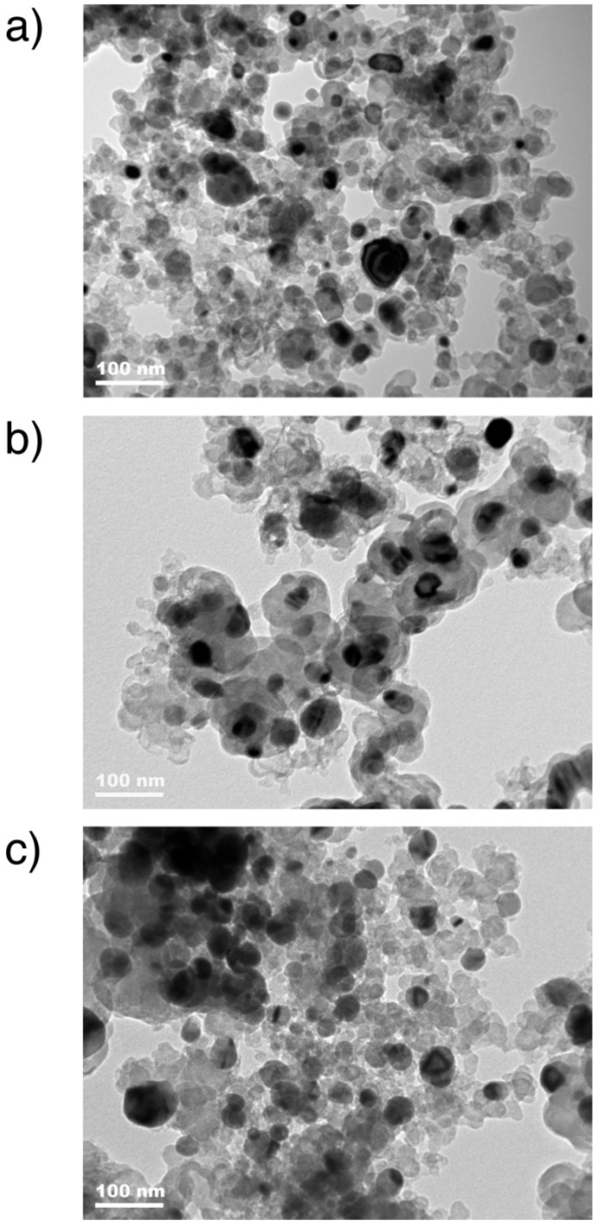

Fig. S5. TEM images of (a) **Fe**/C, (b) **Co**/C, and (c) **Ni**/C.

9.

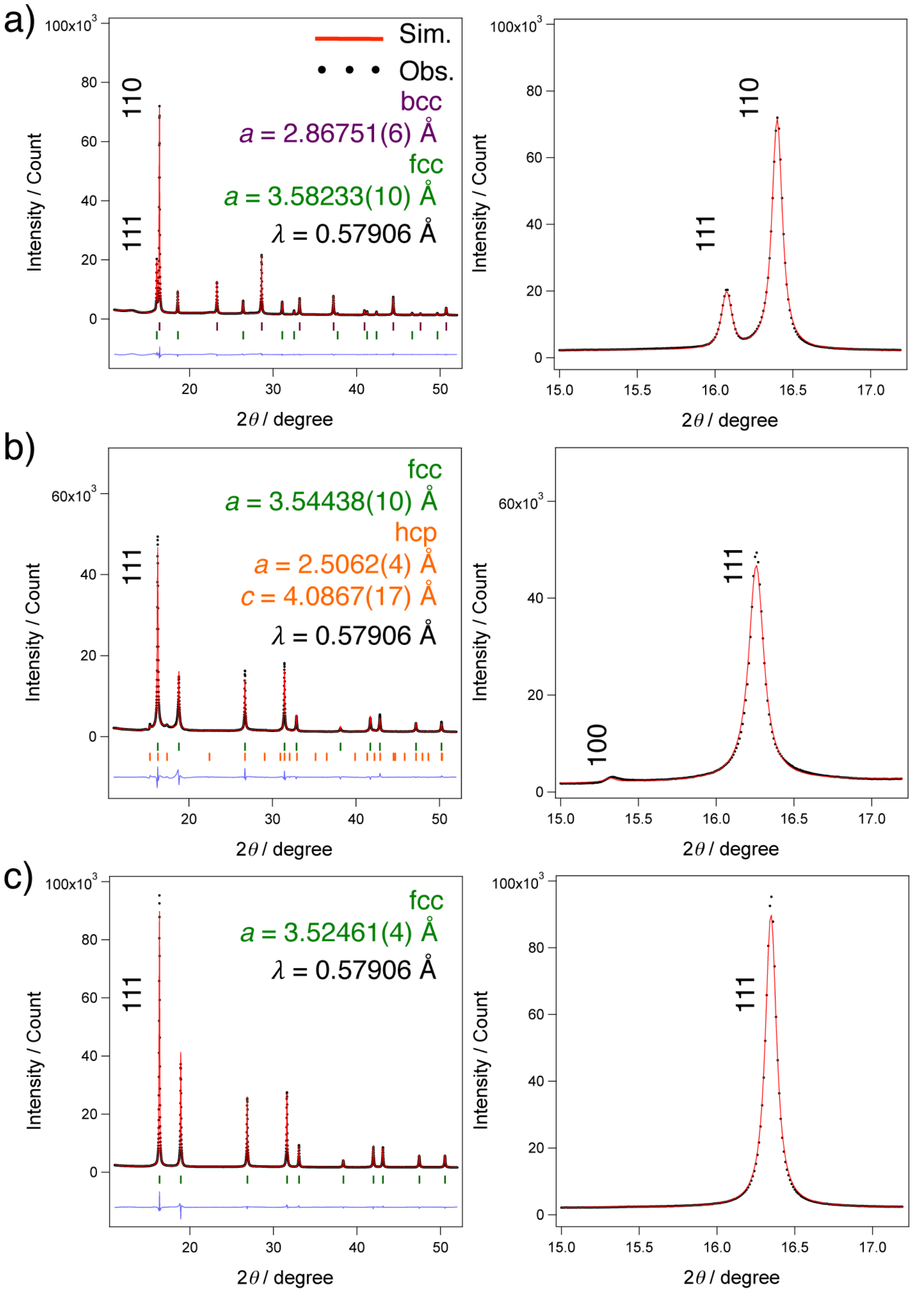

Fig. S6. Powder XRD patterns (black) of (a, left) **Fe**/C, (b, left) **Co**/C, and (c, left) **Ni**/C and and optimized Rietveld profiles (red), with (right) close-up patterns around the lowest angle peaks.

10.

Table S4. Structural parameters of Fe-group NA and monometallic NP catalysts determined by Rietveld analyses.

	FeCoNi/C	**FeCo**/C	**FeNi**/C	**CoNi**/C
Percentage (%)	100	100	100	100
Crystal system	Cubic	Cubic	Cubic	Cubic
Space group	*Fm-3m*	*Im-3m*	*Fm-3m*	*Fm-3m*
a (Å)	3.57418(8)	2.85671(3)	3.53373(12)	3.58464(5)
d (°)	37.2(21)	58.2(4)	30.2(2)	44.4(2)
V (Å^3)	45.659(3)	23.3131(9)	44.127(4)	46.061(2)
T (K)	298	298	298	298
R_p	2.48	2.55	3.51	2.44
R_{WP}	3.37	3.62	5.23	3.34
2θ range	11.0 - 52.0 °	11.0 - 52.0 °	11.0 - 52.0 °	11.0 - 52.0 °
Wavelength (Å)	0.579059	0.579059	0.579059	0.579059

	Fe/C(fcc)	**Fe**/C(bcc)	**Co**/C(fcc)	**Co**/C(hcp)	**Ni**/C
Percentage (%)	24.51	75.49	98.75	1.25	100
Crystal system	Cubic	Cubic	Cubic	Hexagonal	Cubic
Space group	*Fm-3m*	*Im-3m*	*Fm-3m*	$P6_3/mmc$	*Fm-3m*
a (Å)	3.58233(10)	2.86751(6)	3.54438 (10)	2.5062(4)	3.52461(4)
c (Å)				4.0867(17)	
d (°)	51.8(10)	45.5(3)	29.8(2)	43.0(6)	41.8(2)
V (Å^3)	45.972(9)	23.5785(14)	44.527(4)	22.230(12)	43.786(2)
T (K)	298		298		298
R_p	2.74		4.02		2.27
R_{WP}	3.74		5.91		3.29
2θ range	11.0 - 52.0 °		11.0 - 52.0 °		11.0 - 52.0 °
Wavelength (Å)	0.579059		0.579059		0.579059

11.

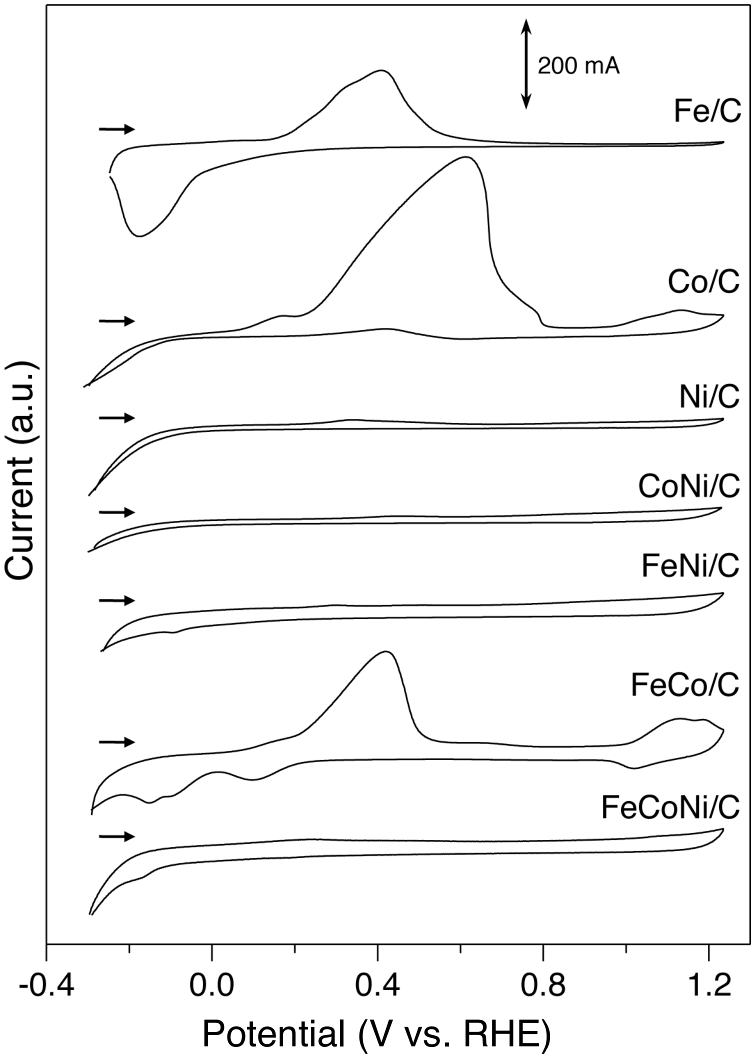

Fig. S7. Blank CVs using **Fe**/C, **Co**/C, **Ni**/C, **CoNi**/C, **FeNi**/C, **FeCo**/C, and **FeCoNi**/C modified working electrodes in 20wt% KOH aqueous solution. Scan rate: 10 mV/s; Counter electrode: Pt wire; Reference electrode: Hg/HgO in 1 M KOH.

12.

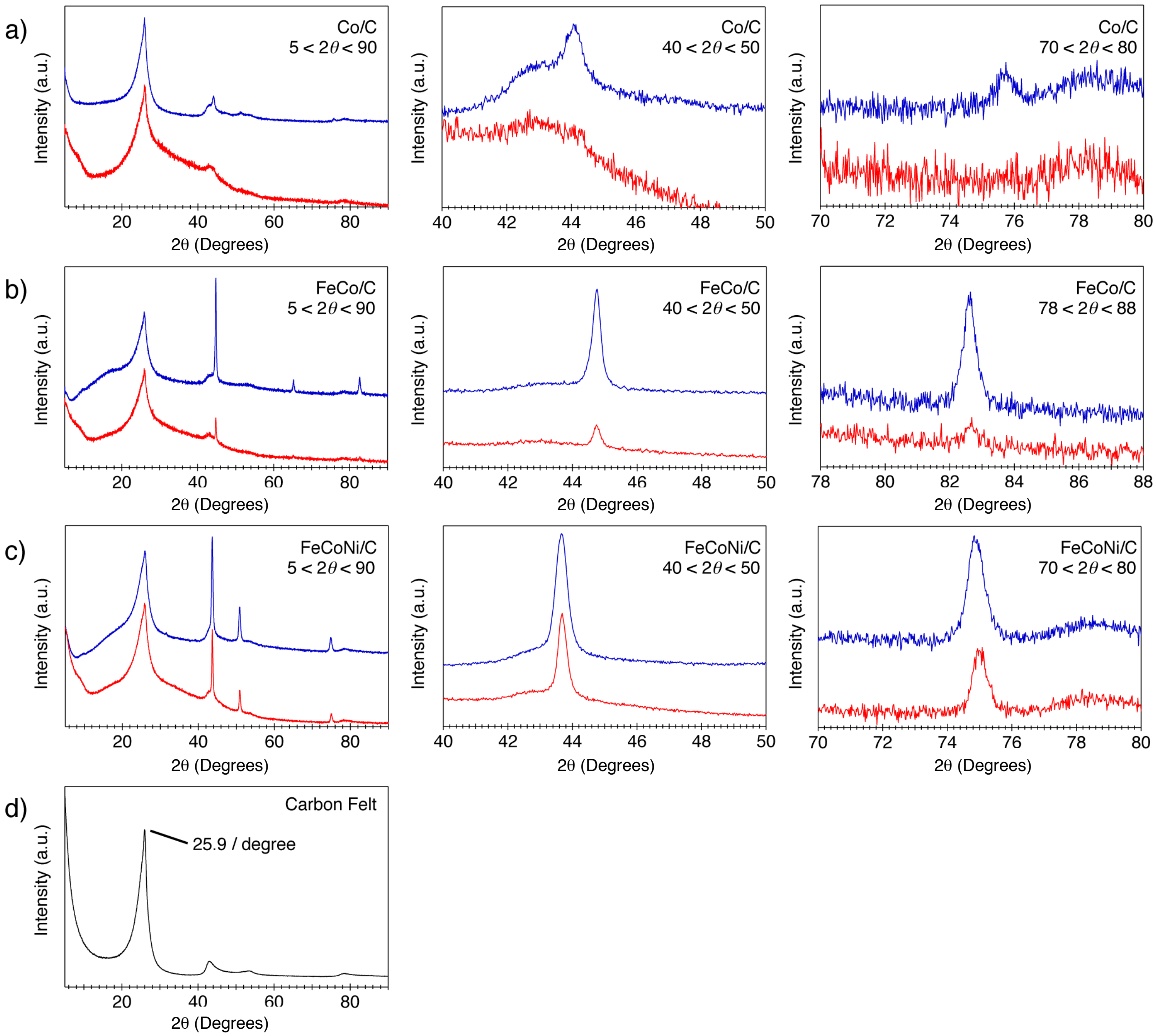

Fig. S8. Powder XRD patterns of (a) **Co**/C, (b) **FeCo**/C and (c) **FeCoNi**/C mounted on carbon felt before (blue line) and after the CA experiment (red line) at 1.0 V (vs. RHE) for 125 min, together with that of (d) carbon felt. Diffraction intensities are normalized to the peak intensity observed at 25.9 degrees for the support.

13.

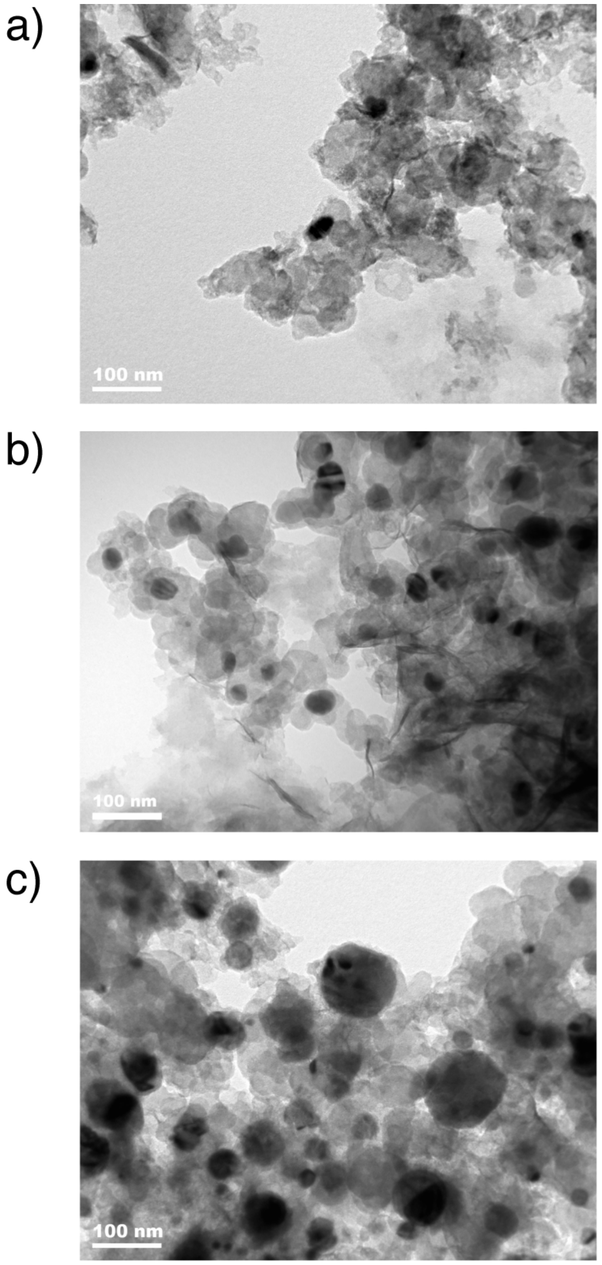

Fig. S9. TEM images of (a) **Co**/C, (b) **FeCo**/C, and (c) **FeCoNi**/C after the CA experiment at 1.0 V (vs. RHE) for 125 min.

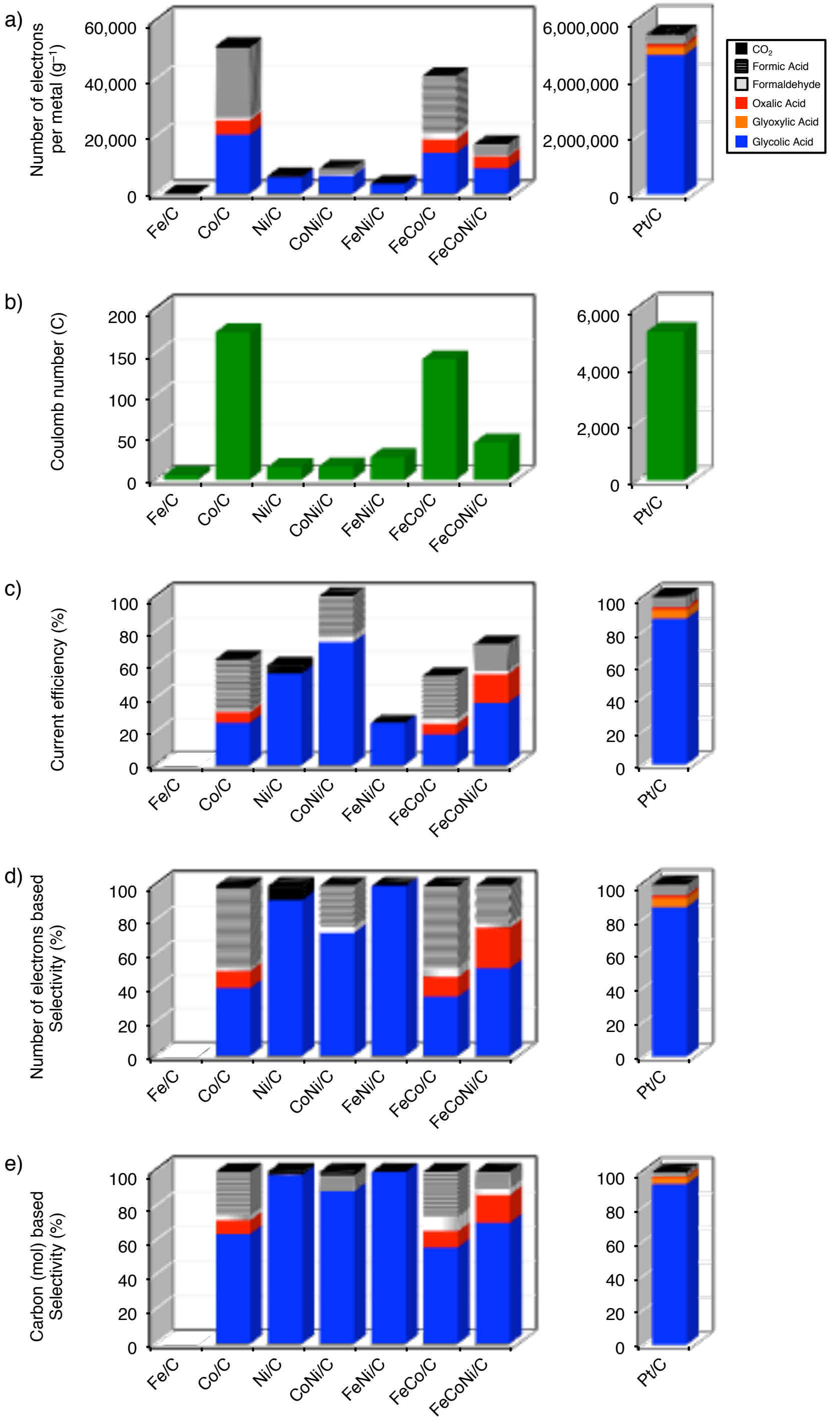

Fig. S10. (a) Number of electrons per metal weight in catalyst, (b) Coulomb number, (c) current efficiency, (d) number of electrons based selectivity, and (d) carbon (mol) based selectivity, related to the oxidized product formation from EG on Fe-group NA and monometallic NP catalysts, together with those of Pt/C counted after 125 min at 1.0 V (vs. RHE).

15.

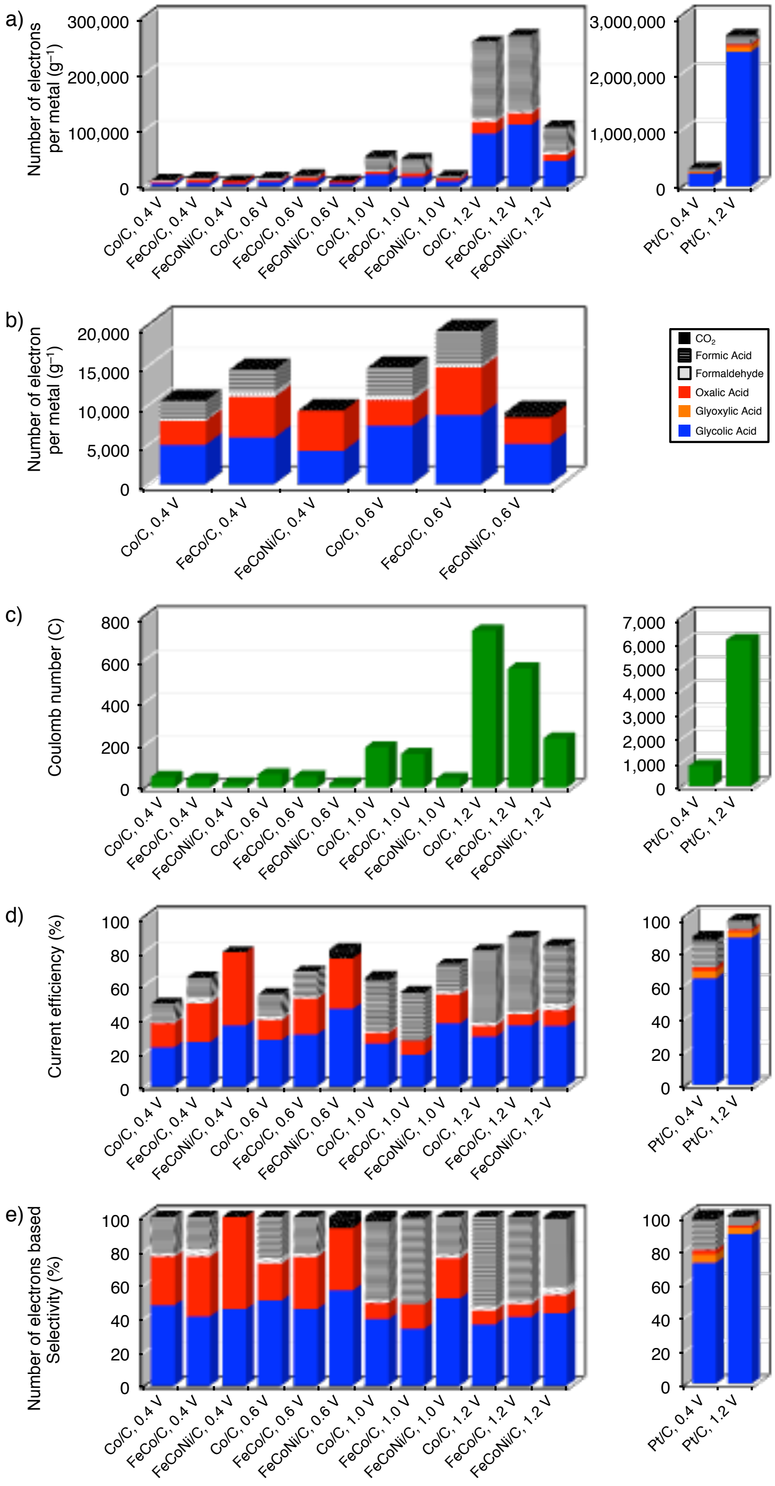

Fig. S11. (a) Number of electrons per metal weight in catalyst, together with (b) those at lower potentials, (c) Coulomb number, (d) current efficiency, and (e) number of electrons based selectivity, related to the oxidized product formation from EG on **Co**/C, **FeCo**/C, and **FeCoNi**/C catalysts, together with those of Pt/C, counted after 125 min at several potentials (0.4, 0.6, 1.0, and 1.2 V vs. RHE).

16.

Table S5. Adsorption energy of glycolic acid on **FeCo**(001) and **FeCoNi**(111) when two oxygen atoms of a glycolic acid molecule are placed on Fe, Co, and Ni atoms. The origin corresponds to the sum of the total energy of an isolated glycolic acid molecule and the isolated surface.

Surface	Adsorption sites of two oxygen atom of a glycolic acid molecule	Adsorption energy (kcal/mol)
FeCo(001)	O/Fe and O/Fe	44.05
	O/Fe and O/Co	37.58
FeCoNi(111)	O/Fe and O/Fe	5.96
	O/Fe and O/Co	5.89
	O/Fe and O/Ni	4.64

* O/Fe means the adsorption of an oxygen atom of a glycolic acid molecule on a Fe atom of **FeCo**(001) or **FeCoNi**(111).

17.

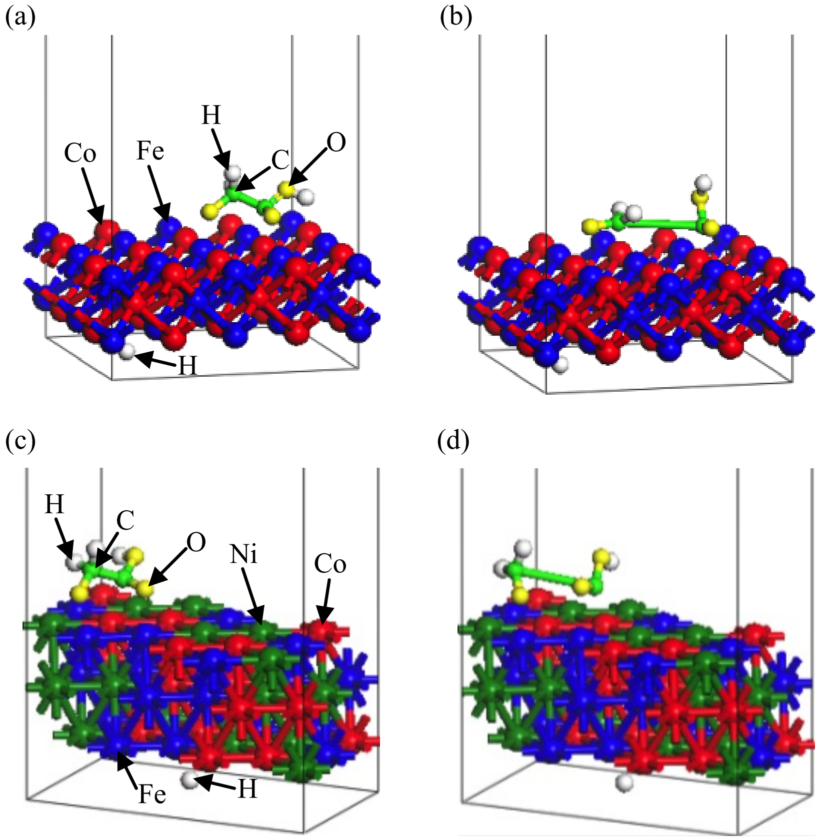

Fig. S12. Adsorption configurations of glycolic acid (a) at an initial state and (b) after C-C bond dissociation on **FeCo**(001), and (c) at the initial state and (d) after C-C bond dissociation on **FeCoNi**(111). For neutralization of the model, a hydrogen atom is placed at bottom of the slab.

18.

Table S6. Charges and C-C bond lengths of a glycolic acid molecule on **FeCo**(001) and **FeCoNi**(111) surfaces at initial, transition, and final states.

Surface		Charge of glycolic acid	C-C bond length (Å)
FeCo(001)	Initial state	-0.468	1.544
	Transition state	-0.346	2.745
	Final state	-0.344	3.819
FeCoNi(111)	Initial state	-0.391	1.538
	Transition state	-0.342	2.488
	Final state	-0.135	4.046

19.

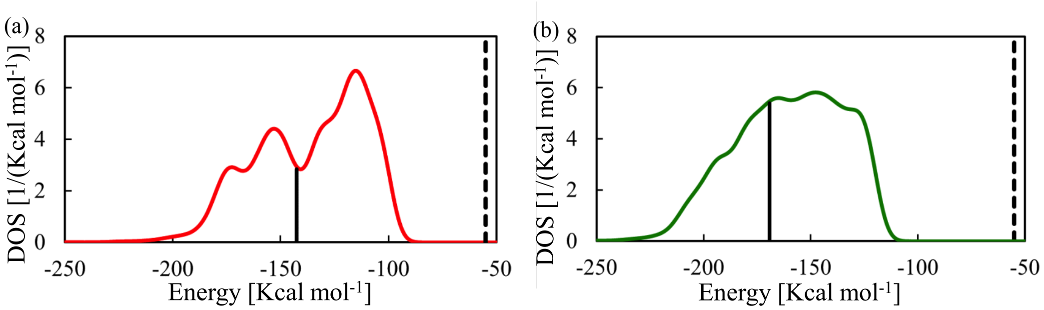

Fig. S13. Density of states (DOS) for (a) FeCo(001) and (b) FeCoNi(111). The vertical dashed line is the energy level of LUMO of glycolic acid. The vertical solid lines corresponds to *d*-band centers of the FeCo(001) and FeCoNi(111) surfaces. The origin of energy corresponds to a vacuum level.

20.

Table S7. Power generation from direct EG FCs using several NA catalyst.

Anode Catalyst	Conditions	Maximum Power Density / mW cm^{-2}	Ref.
FeCoNi/C	20wt% KOH 30wt% EG 70 °C $NaCo_2O_4$ (Cathode)	34 at 0.35 V	This Work
FeCo/C	20wt% KOH 30wt% EG 70 °C $NaCo_2O_4$ (Cathode)	46.2 at 0.33 V	This Work
Fe/C	20wt% KOH 30wt% EG 70 °C $NaCo_2O_4$ (Cathode)	8.8 at 0.25 V	This Work
Co/C	20wt% KOH 30wt% EG 70 °C $NaCo_2O_4$ (Cathode)	34.6 at 0.31 V	This Work
Ni/C	20wt% KOH 30wt% EG 70 °C $NaCo_2O_4$ (Cathode)	21.4 at 0.35 V	This Work
Pt/C	2.0 M NaOH 1.0 M EG 50 °C $FeCuN_2/C$ (Cathode)	71 at 0.27 V	7
Pd(NiZn)/C	2.0 M KOH 5wt% EG 25 °C FeCo/C (Cathode)	24 at 0.17 V	8
Pd(NiZn)/C	2.0 M KOH 5wt% EG 80 °C FeCo/C (Cathode)	95 at 0.23 V	8
Pd/C	2.0 M KOH 5wt% EG 25 °C FeCo/C (Cathode)	12 at 0.13 V	8
Pd/C	2.0 M KOH 5wt% EG 80 °C FeCo/C (Cathode)	65 at 0.19 V	8
Pt/C	4.0 M NaOH 2.0 M EG 20 °C Pt/C (Cathode)	19 at approximately 0.23 V	21
$Pt_{0.45}Pd_{0.45}Bi_{0.1}/C$	4.0 M NaOH 2.0 M EG 20 °C Pt/C (Cathode)	28 at approximately 0.37 V	21
PtRu/C	2.0 M NaOH 1.0 M EG 90 °C Pt/C (Cathode)	9 at approximately 0.35 V	25
PdNi/C	7.0 M KOH 1.0 M EG 60 °C non-platinum Hyper-MEC^{TM} (Cathode)	67 at approximately 0.27 V	44
PdNi/C	1.0 M KOH 1.0 M EG 60 °C non-platinum Hyper-MEC^{TM} (Cathode)	35 at approximately 0.22 V	44

21.

References

1. K. Kato, R. Hirose, M. Takemoto, S. Ha, J. Kim, M. Higuchi, R. Matsuda, S. Kitagawa and M. Takata, *AIP Conf. Proc.*, 2010, **1234**, 875-878.
2. T. Matsumoto, M. Sadakiyo, M. L. Ooi, S. Kitano, T. Yamamoto, S. Matsumura, K. Kato, T. Takeguchi and M. Yamauchi, *Sci. Rep.*, 2014, **4**, 5620.
3. A. J. Bard and L. R. Faulkner, *Electrochemical Methods: Fundamentals and Applications*, John Wiley & Sons, Inc.: New York, 2001.
4. B. Delley, *J. Chem. Phys.*, 2000, **113**, 7756-7764.
5. J. P. Perdew, K. Burke and M. Ernzerhof, *Phys. Rev. Lett.*, 1996, **77**, 3865-3868.
6. K. Miyazaki, T. Matsumiya, T. Abe, H. Kurata, T. Fukutsuka, K. Kojima and Z. Ogumi, *Electrochim. Acta*, 2011, **56**, 7610-7614.
7. L. Xin, Z. Zhang, J. Qi, D. Chadderdon and W. Li, *Appl. Catal. B: Environ.*, 2012, **125**, 85-94.
8. A. Marchionni, M. Bevilacqua, C. Bianchini, Y.-X. Chen, J. Filippi, P. Fornasiero, A. Lavacchi, H. Miller, L. Wang and F. Vizza, *ChemSusChem*, 2013, **6**, 518-528.
9. Y. Kwon, S. C. S. Lai, P. Rodriguez and M. T. M. Koper, *J. Am. Chem. Soc.*, 2011, **133**, 6914-6917.
10. S. C. Chang, Y. Ho and M. J. Weaver, *J. Am. Chem. Soc.*, 1991, **113**, 9506-9513.
11. A. Kumar, *J. Am. Chem. Soc.*, 1981, **103**, 5179-5182.
12. S. Yongprapat, A. Therdthianwong and S. Therdthianwong, *J. Electroanal. Chem.*, 2013, **697**, 46-52.
13. J.-L. Lin, J. Ren, N. Tian, Z.-Y. Zhou and S.-G. Sun, *J. Electroanal. Chem.*, 2013, **688**, 165-171.

14. F. Kosaka, Y. Oshima and J. Otomo, *Electrochim. Acta*, 2011, **56**, 10093-10100.

15. T. Ramulifho, K. I. Ozoemena, R. M. Modibedi, C. J. Jafta and M. K. Mathe, *J. Electroanal. Chem.*, 2013, **692**, 26-30.

16. H. Yue, Y. Zhao, X. Ma and J. Gong, *Chem. Soc. Rev.*, 2012, **41**, 4218-4244.

17. V. Livshits, M. Philosoph and E. Peled, *J. Power Sources*, 2008, **178**, 687-691.

18. A. Serov and C. Kwak, *Appl. Catal. B: Environ.*, 2010, **97**, 1-12.

19. V. Bambagioni, M. Bevilacqua, C. Bianchini, J. Filippi, A. Marchionni, F. Vizza, L. Q. Wang and P. K. Shen, *Fuel Cells*, 2010, **10**, 582-590.

20. R. B. de Lima, V. Paganin, T. Iwasita and W. Vielstich, *Electrochim. Acta*, 2003, **49**, 85-91.

21. L. Demarconnay, S. Brimaud, C. Coutanceau and J. M. Léger, *J. Electroanal. Chem.*, 2007, **601**, 169-180.

22. A. Kelaidopoulou, E. Abelidou, A. Papoutsis, E. K. Polychroniadis and G. Kokkinidis, *J. Appl. Electrochem.*, 1998, **28**, 1101-1106.

23. V. Selvaraj, M. Vinoba and M. Alagar, *J. Colloid Interface Sci.*, 2008, **322**, 537-544.

24. H. Wang, Z. Jusys and R. J. Behm, *J. Electroanal. Chem.*, 2006, **595**, 23-36.

25. R. Chetty and K. Scott, *J. Appl. Electrochem.*, 2007, **37**, 1077-1084.

26. M. Chojak Halseid, Z. Jusys and R. J. Behm, *J. Electroanal. Chem.*, 2010, **644**, 103-109.

27. Y.-Y. Chu, Z.-B. Wang, Z.-Z. Jiang, D.-M. Gu and G.-P. Yin, *J. Power Sources*, 2012, **203**, 17-25.

28. A. Falase, K. Garcia, C. Lau and P. Atanassov, *Electrochem. Commun.*, 2011, **13**, 1488-1491.

29. A. Falase, M. Main, K. Garcia, A. Serov, C. Lau and P. Atanassov, *Electrochim. Acta*, 2012, **66**, 295-301.

30. Y. Feng, W. Yin, Z. Li, C. Huang and Y. Wang, *Electrochim. Acta*, 2010, **55**, 6991-6999.

31. N. Fujiwara, Z. Siroma, T. Ioroi and K. Yasuda, *J. Power Sources*, 2007, **164**, 457-463.

32. Y. Huang, Y. Guo and Y. Wang, *J. Power Sources*, 2014, **249**, 9-12.

33. R. Kannan, K. Karunakaran and S. Vasanthkumar, *Ionics*, 2012, **18**, 803-809.

34. D. Kaplan, M. Alon, L. Burstein, Y. Rosenberg and E. Peled, *J. Power Sources*, 2011, **196**, 1078-1083.

35. D. Kaplan, L. Burstein, Y. Rosenberg and E. Peled, *J. Power Sources*, 2011, **196**, 8286-8292.

36. S.-S. Li, Y.-Y. Hu, J.-J. Feng, Z.-Y. Lv, J.-R. Chen and A.-J. Wang, *Int. J. Hydrogen Energy*, 2014, **39**, 3730-3738.

37. Z. Y. Li, Y. J. Liang, S. P. Jiang, X. D. Shan, M. L. Lin and C. W. Xu, *Fuel Cells*, 2012, **12**, 677-682.

38. R. Ojani, J.-B. Raoof and V. Rahemi, *Int. J. Hydrogen Energy*, 2011, **36**, 13288-13294.

39. A. M. A. Ouf, A. A. Ibrahim and A. A. El-Shafei, *Electroanalysis*, 2011, **23**, 1998-2006.

40. J. Sieben, M. E. Duarte, C. Mayer and J. Bazán, *J. Appl. Electrochem.*, 2009, **39**, 1045-1051.

41. H. Wang, Z. Jusys and R. J. Behm, *Electrochim. Acta*, 2009, **54**, 6484-6498.

42. H. Wang, Y. Zhao, Z. Jusys and R. J. Behm, *J. Power Sources*, 2006, **155**, 33-46.

43. G. Yu, W. Chen, J. Zhao and Q. Nie, *J. Appl. Electrochem.*, 2006, **36**, 1021-1025.

44. L. An, T. S. Zhao, S. Y. Shen, Q. X. Wu and R. Chen, *Int. J. Hydrogen Energy*, 2010, **35**, 4329-4335.